Communications in Applied Analysis, **23**, No. 1 (2019), 61-77 ISSN: 1083-2564

PORO-VISCO-ELASTIC MODELS IN BIOMECHANICS: SENSITIVITY ANALYSIS

LORENA BOCIU[1] AND MARCELLA NOORMAN[2]

[1]Department of Mathematics and
Center for Research in Scientific Computation
North Carolina State University
Raleigh, NC 27695, USA

[2]Department of Mathematics
Center for Research in Scientific Computation
North Carolina State University
Raleigh, NC 27607 USA

ABSTRACT: The main goal of this work is to numerically investigate the sensitivity of biomechanical responses of deformable, porous media to applied external loads. Fluid flows through deformable porous media are relevant for many applications in biology, medicine and bioengineering, like perfusion of tissues in the human body, or fluid flows inside cartilages, bones, and engineered tissue scaffolds. Sensitivity analysis provides valuable insights about how robust the system is with respect to changes in parameters and data and reveals which ones are the most influential for the solutions, and could potentially be used as control agents.

AMS Subject Classification: 35Q74, 35B44

Received: August 19, 2018 ; **Accepted:** December 6, 2018 ;
Published: December 15, 2018 **doi:** 10.12732/caa.v23i1.5
Dynamic Publishers, Inc., Acad. Publishers, Ltd. http://www.acadsol.eu/caa

1. INTRODUCTION

Poro-visco-elastic models provide a good representation of the mechanical characteristics of biological tissues like articular cartilages, bones, and engineered tissue scaffolds, and have been widely used to analyze in vitro creep and stress relaxation experiments on the tissues under confined and unconfined compression tests [6, 9, 12, 14]. The models couple the viscoelastic solid matrix with the interstitial fluid flow through the permeability tensor which is dependent on the solid dilation. Biological tissues have a mass density similar to that of water, so the assumption is that the solid and fluid are incompressible components in the mixture. In most applications, the dynamics of these fluid-solid mixtures are driven by boundary forces (applied external loads) and therefore the investigation of their influence on the biomechanical responses of the coupled systems is of utmost importance.

This issue was recently considered in a series of papers [5, 15]. The first one focused on (i) well-posedness analysis for 3-D poro-elastic and poro-visco-elastic nonlinear systems, and (ii) associated numerical investigation of the corresponding 1-D model. The results highlighted the role of the structural viscosity in lowering the time regularity requirements for the data (volumetric and boundary forcing terms) in comparison to the poro-elastic scenario and provided numerical clues that sudden changes in the data may lead to fluid energy blow-up and micro-structural damage in the absence of structural viscoelasticity. This new hypothesis for tissue micro-structural damage was further investigated in [15]. The response of deformable porous media with incompressible constituents to external applied loads (either step or trapezoidal pulses) and the role that the structural viscosity plays in this response were analyzed for the 1-D prototype. The authors showed that the fluid velocity within the medium could increase tremendously (even up to infinity), should the external applied load experience sudden changes in time and the structural viscoelasticity be too small. Moreover, [15] provided a dimensional analysis of the system and identified some dimensionless parameters that could be used in the design of structural properties and experimental conditions in order to maintain the fluid velocity within the medium below a desired threshold, and implicitly prevent potential damage to the tissue.

In [1, 2], we built upon the results in [5] and performed sensitivity anal-

ysis on the 1-D poro-elastic and poro-visco-elastic solutions with respect to the boundary traction. The viscous component was added in the constitutive stress-strain relation for the solid in the form of $\delta \frac{\partial^2 u}{\partial t \partial x}$, where the parameter $\delta = \lambda_v + 2\mu_v$ indicated the extent to which the model included viscoelastic effects for the solid component, with $\delta = 0$ corresponding to the purely elastic case. We found that the effects of the boundary source of traction were most significant for the discharge velocity, especially in the $\delta = 0$ case. This was very much in agreement with the numerical investigation in [5], which hinted that the fluid energy (which is dependent on the discharge velocity) becomes unbounded as the boundary source of traction loses smoothness in time and visco-elasticity is no longer present. Overall, we concluded that the boundary traction can be used as a control parameter for both the fluid pressure and discharge velocity. In comparison, the solid displacement was the least sensitive to boundary data in both elastic and viscoelastic scenarios. This suggested that small changes in displacement may actually correspond to large changes in fluid pressure and discharge velocity, and thus solely monitoring the solid displacement of the material may not be indicative of the fluid-dynamical state inside the medium. Further, if one's main interest is in controlling the solid displacement, then it would be more effective to act on the material elastic and visco-elastic properties rather than the boundary traction. Overall, our numerical results in [1, 2] showed that the solution (solid displacement, fluid pressure and discharge velocity) was more sensitive to boundary traction in the elastic case than in the visco-elastic scenario. Based on the observations mentioned above, we expected to see a direct correlation between the sensitivities and the viscous effects present in the solid component (quantified by δ). However, the numerical sensitivities were not monotonic with respect to the amount of structural viscosity included and rather exhibited complex behavior in space and time. This result prompted the need for dimensional analysis, where relevant physical and geometrical parameters of the problem are combined in dimensionless numbers that can be used to establish some equivalences between behaviors of apparently different systems [15].

In this work, we complement the results from [15] by numerically investigating the sensitivities of the 1-D dimensionless poro-visco-elastic solutions to applied boundary loads and their dependence on the dimensionless parameters identified in [15].

2. PDE MODEL

We consider the 1-D poro-visco-elastic model under the assumptions of small deformations, full saturation of the mixture, incompressibility of the mixture constituents, negligible inertia, and zero volumetric sources of linear momentum and fluid mass [15]. The PDE system is given by

$$\frac{\partial \sigma}{\partial x} = 0 \qquad \text{in } (0,L)\times(0,T) \tag{2.1}$$

$$\frac{\partial \zeta}{\partial t} + \frac{\partial v}{\partial x} = 0 \qquad \text{in } (0,L)\times(0,T) \tag{2.2}$$

$$u(0,t) = 0 \qquad t \in (0,T) \tag{2.3}$$

$$v(0,t) = 0 \qquad t \in (0,T) \tag{2.4}$$

$$\sigma(L,t) = -P(t) \qquad t \in (0,T) \tag{2.5}$$

$$p(L,t) = 0 \qquad t \in (0,T) \tag{2.6}$$

$$u(x,0) = 0 \qquad x \in (0,L) \tag{2.7}$$

where σ is the total stress of the mixture, ζ is the fluid content, v is the discharge velocity, u is the solid displacement, p is the fluid pressure, and $-P(t)$ is the boundary traction. The equations (2.1) and (2.2) represent the balance of linear momentum for the fluid-solid mixture and balance of mass of the fluid component, respectively.

The stress σ is comprised of the elastic stress σ_e, visco-elastic stress σ_v, and pressure p, and is given by

$$\sigma = \underbrace{(\lambda_e + 2\mu_e)\frac{\partial u}{\partial x}}_{\sigma_e} + \underbrace{(\lambda_v + 2\mu_v)\frac{\partial^2 u}{\partial t \partial x}}_{\sigma_v} - p \tag{2.8}$$

where λ_e, μ_e and λ_v, μ_v are the Lamé elastic and visco-elastic parameters respectively.

Due to the assumption of incompressibility of the fluid and solid components of the mixture, the fluid content equals the dilation of the solid, i.e.,

$$\zeta = \frac{\partial u}{\partial x}. \tag{2.9}$$

By Darcy's law, the constitutive equation for the discharge velocity is given by

$$v = -K\frac{\partial p}{\partial x} \tag{2.10}$$

where $K = K(\frac{\partial u}{\partial x})$ is the permeability, whose structure depends on the geometrical architecture of the pores and the physical properties of the fluid. In biological applications, K often depends nonlinearly on $\frac{\partial u}{\partial x}$, resulting in a nonlinear coupling of the balance equations. However, in this paper we will focus on the case $K = K_0$ constant, just like in [15].

As we mentioned in the introduction, we studied the sensitivity of the solutions of the system (2.1)-(2.6) with respect to boundary traction in [1, 2]. In particular, we looked at how varying the amount of viscous effects being included in the solid component (quantified by the viscoelastic parameter $\delta = \lambda_v + 2\mu_v$) affected these sensitivities. We found that the sensitivities as functions of δ often exhibited complex behaviors in space and time and concluded that δ was not a good control parameter for the system. For this reason, in this work we perform sensitivity analysis on a dimensionless version of the model (2.1)-(2.6), which may highlight more clearly which physical and geometrical parameters of the problem will act as good control parameters.

Following [15], we define the dimensionless (or scaled) variables to be

$$\hat{x} = \frac{x}{[x]}, \quad \hat{t} = \frac{t}{[t]}, \quad \hat{P} = \frac{P}{[P]}, \quad \hat{\sigma} = \frac{\sigma}{[\sigma]}, \quad \hat{u} = \frac{u}{[u]}, \quad \hat{v} = \frac{v}{[v]}, \quad \hat{p} = \frac{p}{[p]}.$$

The bracket notation used above denotes the characteristic value for the respective variable. We note that the choice of characteristic values is not trivial and, in general, characteristic values are not unique. In this work, we select the characteristic values found in [15], which are given by

$$[x] = L, \quad [t] = \frac{L^2}{K_0\mu}, \quad [P] = P_{ref}, \quad [\sigma] = P_{ref}$$

$$[u] = \frac{P_{ref}L}{\mu}, \quad [v] = \frac{K_0 P_{ref}}{L}, \quad [p] = P_{ref}$$

where P_{ref} is a reference value, for example the mean value of the given function $P(t)$.

For $\hat{T} = \frac{T}{[t]}$, the dimensionless system is then given by

$$\frac{\partial \hat{\sigma}}{\partial \hat{x}} = 0 \qquad \text{in } (0,1) \times (0,\hat{T}) \tag{2.11}$$

$$\frac{\partial^2 \hat{u}}{\partial \hat{t} \partial \hat{x}} + \frac{\partial \hat{v}}{\partial \hat{x}} = 0 \qquad \text{in } (0,1) \times (0,\hat{T}) \tag{2.12}$$

$$\hat{u}(0,\hat{t}) = 0 \qquad \hat{t} \in (0,\hat{T}) \tag{2.13}$$

$$\hat{v}(0,\hat{t}) = 0 \qquad \hat{t} \in (0,\hat{T}) \tag{2.14}$$

$$\hat{\sigma}(1,\hat{t}) = -\hat{P}(\hat{t}) \qquad \hat{t} \in (0,\hat{T}) \tag{2.15}$$

$$\hat{p}(1,\hat{t}) = 0 \qquad \hat{t} \in (0,\hat{T}) \tag{2.16}$$

$$\hat{u}(\hat{x},0) = 0 \qquad \hat{x} \in (0,1) \tag{2.17}$$

with constitutive equations

$$\hat{\sigma} = \frac{\partial \hat{u}}{\partial \hat{x}} + \hat{\eta}\frac{\partial^2 \hat{u}}{\partial \hat{t}\partial \hat{x}} - \hat{p} \tag{2.18}$$

$$\hat{v} = -\frac{\partial \hat{p}}{\partial \hat{x}} \tag{2.19}$$

The parameter $\hat{\eta}$ in (2.18), given by

$$\hat{\eta} = \frac{L^2}{K_0}(\lambda_v + 2\mu_v), \tag{2.20}$$

is the analog to the viscoelastic parameter δ used in [1, 2, 5], with $\hat{\eta} = 0$ corresponding to $\delta = 0$, which is the poro-elastic case.

The solution to the dimensionless system was found in [15] to be

$$\hat{u}(\hat{x},\hat{t}) = -2\sum_{n=0}^{\infty} \frac{(-1)^n y_n(\hat{x})}{1+\hat{\eta}\hat{\lambda}_n} \exp\left(-\frac{\hat{\lambda}_n}{1+\hat{\eta}\hat{\lambda}_n}\hat{t}\right) * \hat{P}(\hat{t}) \tag{2.21}$$

$$\hat{p}(\hat{x},\hat{t}) = 2\sum_{n=0}^{\infty} \frac{(-1)^n y_n'(\hat{x})}{\sqrt{\hat{\lambda}_n}(1+\hat{\eta}\hat{\lambda}_n)} \left[\hat{P}(\hat{t}) - \frac{\hat{\lambda}_n}{1+\hat{\eta}\hat{\lambda}_n} \exp\left(-\frac{\hat{\lambda}_n}{1+\hat{\eta}\hat{\lambda}_n}\hat{t}\right) * \hat{P}(\hat{t})\right] \tag{2.22}$$

$$\hat{v}(\hat{x},\hat{t}) = 2\sum_{n=0}^{\infty} \frac{(-1)^n y_n(\hat{x})}{1+\hat{\eta}\hat{\lambda}_n} \left[\hat{P}(\hat{t}) - \frac{\hat{\lambda}_n}{1+\hat{\eta}\hat{\lambda}_n} \exp\left(-\frac{\hat{\lambda}_n}{1+\hat{\eta}\hat{\lambda}_n}\hat{t}\right) * \hat{P}(\hat{t})\right] \tag{2.23}$$

$$\hat{\sigma}(\hat{x},\hat{t}) = -\hat{P}(\hat{t}) \tag{2.24}$$

where $'$ denotes ordinary differentiation, $*$ denotes convolution, and, for $n = 0, 1, \ldots,$

$$\hat{\lambda}_n = \frac{(2n+1)^2\pi^2}{4}, \tag{2.25}$$

$$y_n(\hat{x}) = \sin\left(\sqrt{\hat{\lambda}_n}x\right). \tag{2.26}$$

For well-posedness results on the dimensionless system, see [15].

3. NUMERICAL SOLUTION

The system was solved numerically using the approach outlined in [2, 5]. The algorithm is comprised of a backward Euler discretization in time and a dual mixed hybridized (DMH) finite element discretization in space. The DMH finite element algorithm treats both the primal variables $\hat{u}$, $\hat{p}$ and the dual variables $\hat{v}, \hat{\sigma}$ as independent variables. The DMH finite element solutions $\hat{u}_h, \hat{p}_h$ are further restricted to the interior of the elements and the approximation of their values at the spatial nodes are treated as separate variables $\underline{\hat{u}_h}, \underline{\hat{p}}_h$. One might intuitively think that the introduction of so many variables would increase computation time adversely. However, the equations resulting from this algorithm are mostly local and as such an elimination procedure called static condensation can be used to eliminate $\hat{u}_h, \hat{p}_h, \hat{v}_h, \hat{\sigma}_h$ in favor of the nodal variables $\underline{\hat{u}}_h$,$\underline{\hat{p}}_h$ and the problem data.

The resulting solution was validated against the series approximations (2.21)-(2.23). The norm used to measure the difference of the approximated solution with the series approximation is given by

$$\|w\|_Q := \sup_{t\in[0,\hat{T}]} \|w(t)\|_{L^2(0,1)} \tag{3.1}$$

for any function $w(x,t)$. Using this norm, we found that our algorithm consistently gives solutions within 10^{-5} of the series approximation.

4. SENSITIVITY ANALYSIS

Our main objective is to determine the sensitivity of $(\hat{u}, \hat{p}, \hat{v})$ with respect to the boundary traction $\hat{P}$ and observe how the value of $\hat{\eta}$ affects these sensitivities. This, in essence, amounts to computing the sensitivity matrix $\frac{\partial(\hat{u},\hat{p},\hat{v})}{\partial \hat{P}}$ for many different values of $\hat{\eta}$. In this case, since the series solution is known and the system is linear, we can compute series representations of the sensitivities analytically. However, if we allow permeability to be nonlinear (which is the next step in this analysis), we will need to use computational methods in order to obtain approximate sensitivities.

The following simulations were done using the complex step method to compute the sensitivities [3, 4, 7, 8, 10, 11]. This method utilizes complex anal-

ysis in a clever way to approximate derivatives without any type of cancellation error. The complex-step derivative approximation is given by $\frac{\partial f}{\partial x} \approx \frac{\mathrm{Im}[f(x+ih)]}{h}$, for small step size parameter h (up to machine precision). The complex-step estimate is very accurate and extremely robust in numerical computations, while retaining a reasonable computational cost [3, 4]. The main advantage of this method is that the complexity of the algorithm is the same as the complexity of the algorithm that solves the system of equations. For complete details on the complex step method see [3] and the references therein. In our case, due to the linearity of the system, the complex step method is equivalent to numerically solving the sensitivity system. Series approximations to the sensitivities (which we obtained using (2.21)-(2.23)) were also used to validate the results. This suggests that the complex step method may be an appropriate method for computing sensitivities in the case of nonlinear permeability. Thus, our work here both studies the sensitivity of the system in the case of constant permeability and provides evidence for the use of the complex step method when the permeability is a nonlinear function of dilation.

In order to numerically approximate the functional derivative $\frac{\partial \hat{u}}{\partial \hat{P}}$ ($\frac{\partial \hat{p}}{\partial \hat{P}}$, $\frac{\partial \hat{v}}{\partial \hat{P}}$ respectively) we approximate $\hat{P}$ with linear splines $s_1, \ldots, s_n$ giving us

$$\hat{P}(\hat{t}) \approx \tilde{P}(\hat{t}) = \sum_{i=1}^{n} \alpha_i s_i(\hat{t}) \tag{4.1}$$

for some constants α_i, $i = 1, \ldots, n$. We then use the complex step method to compute the derivatives of $\hat{u}$ ($\hat{p}, \hat{v}$ respectively) with respect to the coordinates α_i of $\tilde{P}$ in the linear spline space in order to construct the Jacobian matrix of $\hat{u}$ ($\hat{p}, \hat{v}$ respectively) with respect to $\alpha = [\alpha_1, \ldots, \alpha_n]^T$. For a given direction $\bar{P} \in \mathrm{span}\{s_1, \ldots, s_n\}$, it can be seen that this matrix acts as an approximation of the action of the functional derivative on $\bar{P}$ through the chain rule for Gateaux derivatives [1, 2].

5. RESULTS

In this section, we look at the sensitivities of $\hat{u}, \hat{p}$, and $\hat{v}$ with respect to $\hat{P}$ in the direction of the linear splines shown in Figure 1. In particular, we display here the sensitivities of $\hat{u}$ in the direction of s_2 (Figure 1, middle panel) and

the sensitivities of $\hat{p}, \hat{v}$ in the direction s_1 (Figure 1, left panel). We note that the behaviors shown and discussed here are typical of the sensitivities for the other splines as well. Understanding the behavior of the sensitivities in the direction of these splines unveils how the sensitivities will behave in any direction that can be accurately approximated by linear splines.

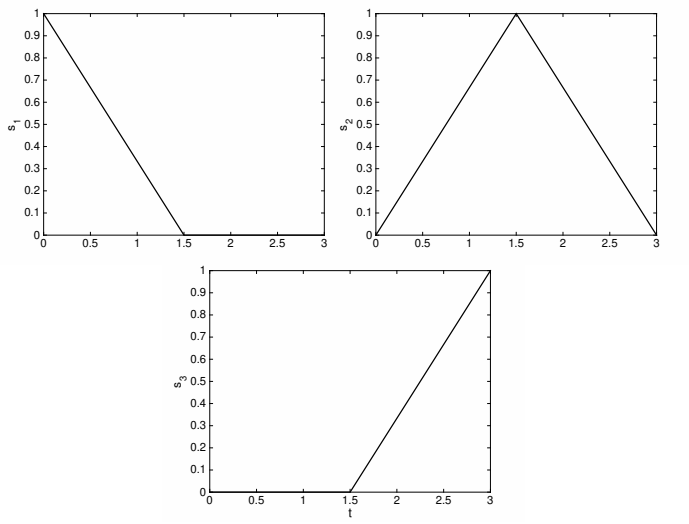

Figure 1: Linear splines

General Comments. We note the following common trend: the sensitivity curves (for all three variables $\hat{u}$, $\hat{p}$ and $\hat{v}$) appear to follow similar behaviors regardless of the value of $\hat{\eta}$, except for times that are really close to $\hat{t} = 0$. Away from $\hat{t} = 0$, the two main differences (with respect to $\hat{\eta}$) between the sensitivity curves appear to be their maximum magnitude and the rate at which they react to changes in the slope of $\bar{P}$. For the magnitudes of the sensitivities, we do see that the maximum is monotonic with respect to $\hat{\eta}$, with smaller values of $\hat{\eta}$ resulting in larger maximum magnitudes. This monotonicity in magnitudes, however, is not true over all time and space. Rather, we see that for smaller values of $\hat{\eta}$, the sensitivities tend to react more quickly to changes in the slope of $\bar{P}$ which causes the sensitivities for different values of $\hat{\eta}$ to "cross over" each other. In fact, it appears that there is a "lag" in the sensitivities for larger values of $\hat{\eta}$ which visually manifests itself in the appearance of the sensitivity curves for smaller values of $\hat{\eta}$ "leading" the sensitivity curves for larger values of $\hat{\eta}$ in monotonic order.

On the other hand, near time $\hat{t} = 0$ the sensitivities show drastically different behavior depending upon whether $\hat{\eta} = 0$ or $\hat{\eta} > 0$. This is particularly true for the sensitivities of $\hat{p}$ and $\hat{v}$ when $\hat{\eta} = 0$, which show discontinuities and blow up (respectively) near the boundary $\hat{x} = 1$ where the boundary traction is imposed. This is discussed in more detail below.

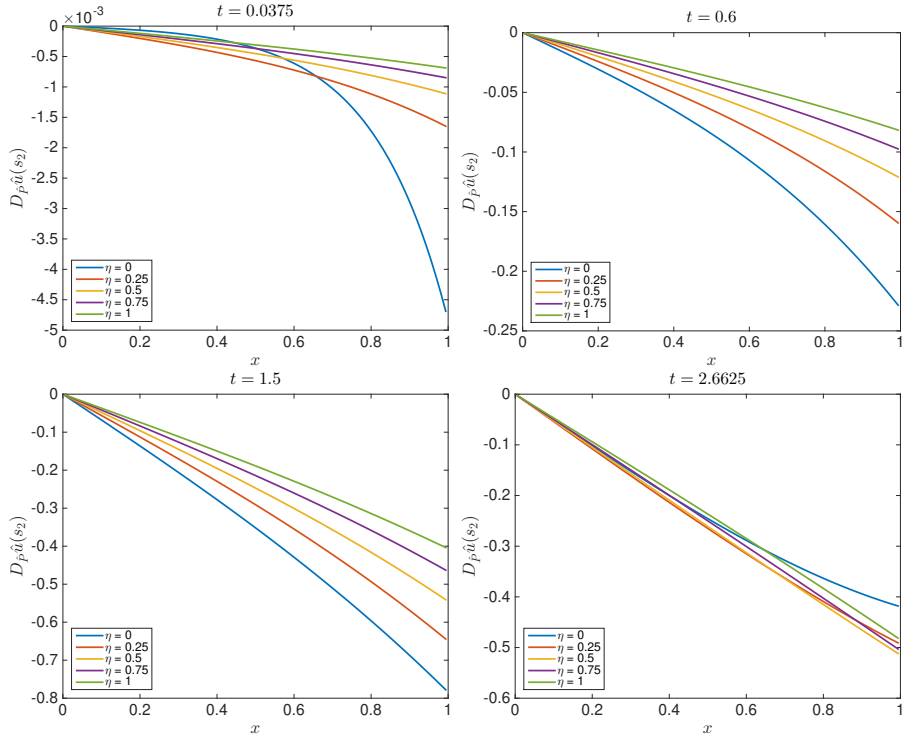

Figure 2: Sensitivity of $\hat{u}$ to $\hat{P}$ in direction $s_2(t)$ for $0 \leq \eta \leq 1$

Sensitivity of the solid displacement $\hat{u}$. Figure 2 shows the sensitivities of $\hat{u}$ in the direction $\bar{P} = s_2$ at some conveniently selected times $\hat{t}$, for various values of $\hat{\eta} \in [0, 1]$. We chose this particular snapshots to include specific times when the slope of $\bar{P}$ is constant (either positive or negative), as well as changing, and show the behavior of the sensitivities in those scenarios. In general, we found that the magnitude of the sensitivity of $\hat{u}$ with respect to $\hat{P}$ depends mostly upon the magnitude of $\bar{P}$. While $\bar{P}$ is increasing away from zero, we see the magnitudes of the sensitivities of $\hat{u}$ increasing as well. Similarly, when $\bar{P}$ starts decreasing back to zero, we see the magnitudes of the sensitivities of $\hat{u}$ decrease as well, though there is a slight lag in their response

which is proportional to the value of $\hat{\eta}$.

Note that the bottom right panel of Figure 2 shows the crossing over of the sensitivities due to the change in slope of $\bar{P}$ from positive to negative. This is due to a lag in the reaction of the sensitivities to this change of slope (which occurs at $\hat{t} = 1.5$) for $\hat{\eta} > 0$. To illustrate this lag further, we plot the maximum value of the magnitude of the sensitivity of $\hat{u}$ in the direction s_2 against the time at which it occurs in Figure 3a. Here, we see that smaller values of $\hat{\eta}$ indeed lead to sensitivities with larger magnitudes, which are obtained in shorter time spans. This corresponds to the lag we see in Figure 2 in sensitivities with larger $\hat{\eta}$ values.

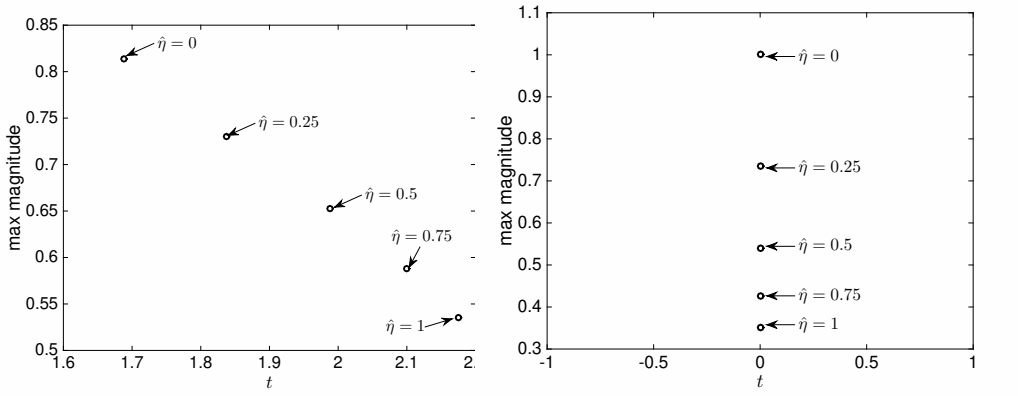

(a) Maximum magnitude of $D_{\hat{P}}\hat{u}(s_2)$. (b) Maximum magnitude of $D_{\hat{P}}\hat{p}(s_1)$.

Figure 3: Maximum magnitude of sensitivities and the time at which it occurs for each value of $\hat{\eta}$ considered.

Sensitivity of the pressure $\hat{p}$: In Figure 4, we show the sensitivities of $\hat{p}$ in the direction $\bar{P} = s_1$ for various values of $\hat{\eta} \in [0, 1]$. Overall, we see that $\hat{p}$ is most sensitive when the direction $\bar{P}$ has nonzero slope. When $\bar{P}$ is constant, the sensitivities of $\hat{p}$ collapse to 0. Overall, it appears that, for the most part, when the slope of $\bar{P}$ is nonzero we have larger sensitivities for smaller values of $\hat{\eta}$. When the slope of $\bar{P}$ is zero, the sensitivities for smaller values of $\hat{\eta}$ collapse more quickly causing the sensitivity curves for various values of $\hat{\eta}$ to cross over each other similar to the sensitivities of $\hat{u}$.

Interestingly, while we do see that the senstivities of $\hat{p}$ for larger values of $\hat{\eta}$ react more slowly to changes in the direction $\bar{P}$, the time at which the sensitivities attain their maximum is the same for all $\hat{\eta}$ (see Figure 3b). This

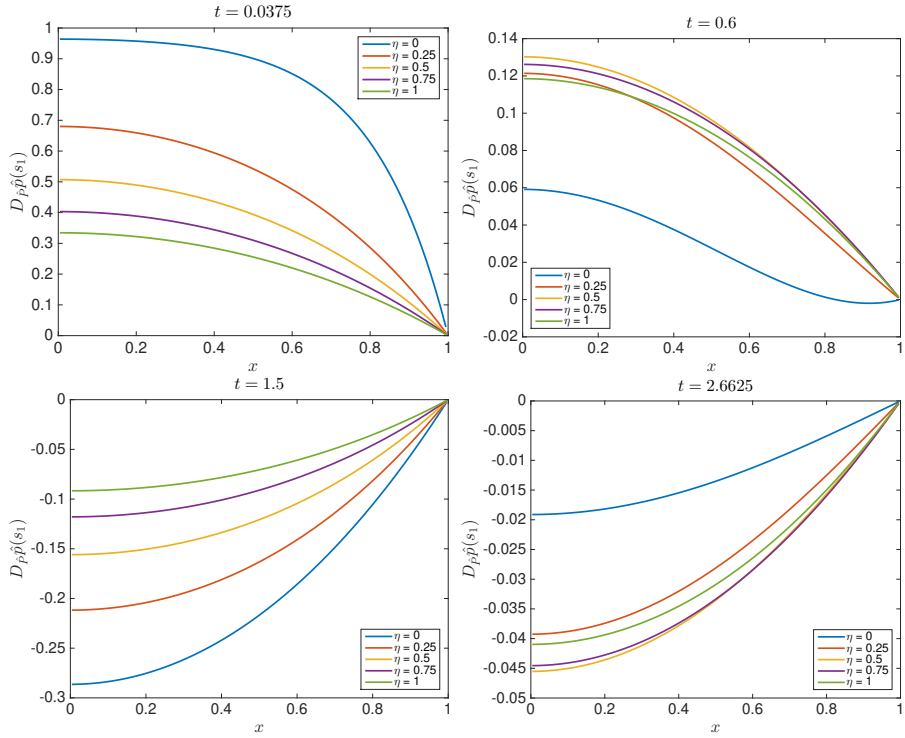

Figure 4: Sensitivity of $\hat{p}$ to $\hat{P}$ in direction $s_1(t)$ for $0 \leq \eta \leq 1$.

indicates that, unlike the sensitivities of the solid displacement $\hat{u}$, the sensitivities of $\hat{p}$ are not exhibiting a true lag in reaction time. Rather, the response of the sensitivities of $\hat{p}$ to a change in $\bar{P}$ is simply smaller for larger $\hat{\eta}$. To investigate this further, we computed the time derivative of the sensitivities using a central finite difference. Figure 5 shows the results at $\hat{x} = 0$ for $\hat{p}$ (left panel) and at $\hat{x} = 1$ for $\hat{v}$ (right panel). Note that the value of $\hat{x}$ was chosen to correspond with where we see the largest changes in the magnitude of these sensitivities. These plots show that the sensitivities do appear to respond at the same time, however the response when $\hat{\eta} = 0$ is much larger than the rest and in general smaller $\hat{\eta}$ corresponds to a larger response.

Sensitivity of the velocity $\hat{v}$: Figure 6 shows the sensitivities of $\hat{v}$ in the direction $\bar{P} = s_1$ for various values of $\hat{\eta} \in [0, 1]$. In general, we see that the sensitivities of $\hat{v}$ are similar to the sensitivities of $\hat{p}$ in that they are most sensitive when the slope of $\bar{P}$ is nonzero and collapse when the slope of $\bar{P}$ is zero. We also see here that the senstivities attain their maximum magnitude

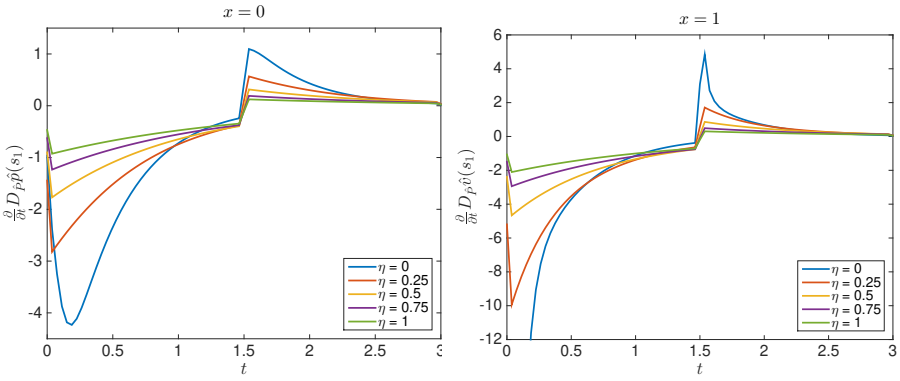

Figure 5: Time derivative of sensitivity of $\hat{p}$ (left panel) and $\hat{v}$ (right panel) in direction s_1.

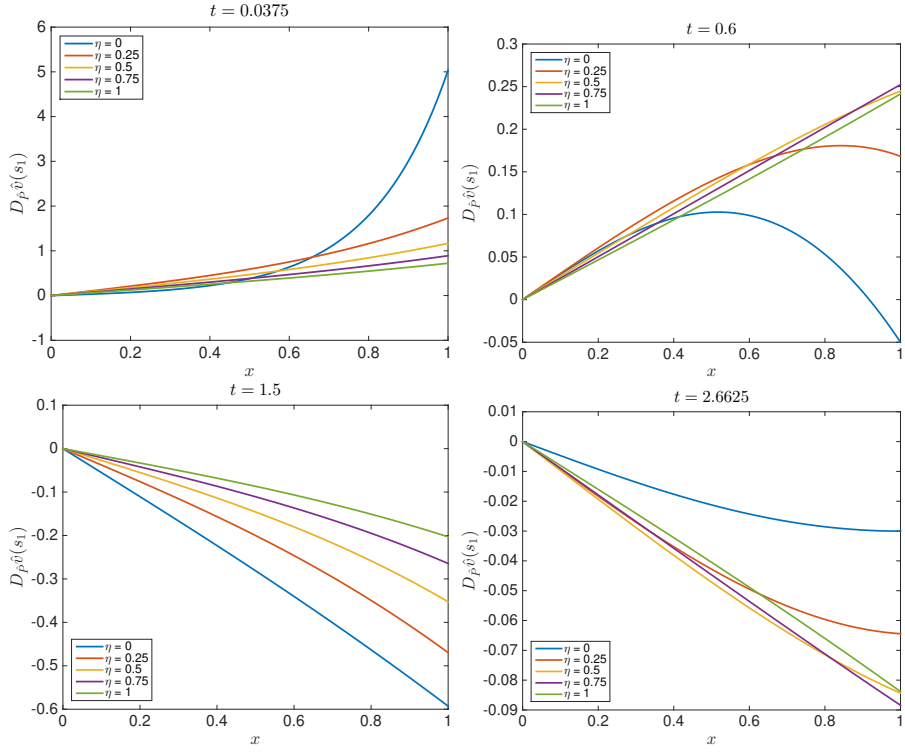

Figure 6: Sensitivity of $\hat{v}$ to $\hat{P}$ in direction $s_1(t)$ for $0 \leq \eta \leq 1$.

at the same time and that that magnitude is larger for smaller values of $\hat{\eta}$.

Sensitivity at $\hat{t} = 0$: When $\hat{\eta} = 0$ and $\hat{t}$ is close to 0 the sensitivities can display some complex and irregular behavior. The behavior here is of

particular interest since, as is noted in [15], the discharge velocity experiences blow up at $\hat{t} = 0$ in the purely elastic case of $\hat{\eta} = 0$. Here, we see that at $\hat{t} = 0$ and for $\hat{\eta} = 0$ the sensitivity of $\hat{p}$ experiences a discontinuity at $\hat{x} = 1$ (note the boundary condition on $\hat{p}$ at $\hat{x} = 1$ is a homogeneous Dirichlet condition) and the sensitivity of $\hat{v}$ blows up at $\hat{x} = 1$. These sensitivities are shown in Figure 7. Note that the log of the sensitivity of $\hat{v}$ (right panel) is shown to better illustrate the blow up.

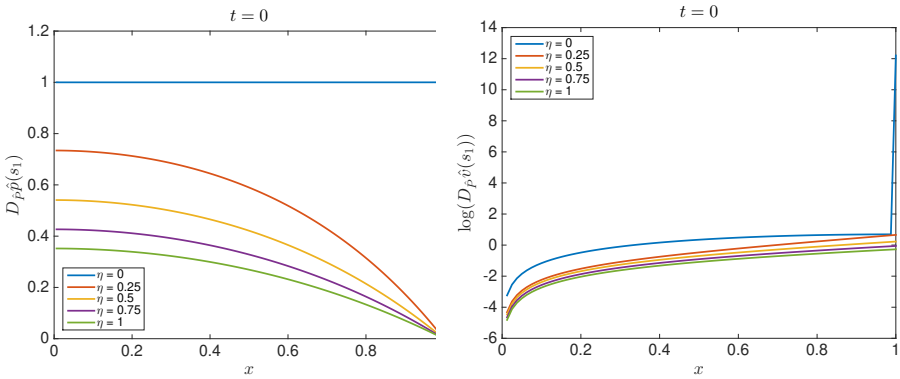

Figure 7: Sensitivity of $\hat{p}$ (left panel) and log of sensitivity of $\hat{v}$ (right panel) with respect to $\hat{P}$ in direction s_1 at time $t = 0$.

6. CONCLUSIONS AND FUTURE WORK

Our results consistently show that the maximum magnitude of the sensitivities (for all three variables $\hat{u}$, $\hat{p}$ and $\hat{v}$) is largest when $\hat{\eta} = 0$ and gets smaller monotonically with respect to $\hat{\eta}$. However, the magnitudes of the sensitivities were not always monotonic with respect to $\hat{\eta}$ and this is due to the response of the sensitivities to changes in the slope of $\bar{P}$ also being dependent upon $\hat{\eta}$. In general, we found that the sensitivities of the solid displacement experience a lag to changes in the slope of $\bar{P}$ if $\hat{\eta} > 0$ with larger values of $\hat{\eta}$ corresponding to longer lag times. On the other hand, while the sensitivities of the fluid pressure and discharge velocity did not experience any lags in time, their responses to changes in the slope of $\bar{P}$ were markedly smaller for larger values of $\hat{\eta}$.

These results correspond closely with results typically observed in creep tests for poro-visco-elastic materials. The lag in the solid displacement due to

the inclusion of structural viscosity is indicative of the increase in time that it takes for the solid to reach an equilibrium after an applied load [9]. The sharp increase in the sensitivity of the fluid pressure when the slope of the direction $\bar{P}$ changes is itself consistent with the phenomena of fluid load support in the early time response of confined compression creep tests [13]. Further, the sensitivities of the fluid pressure collapse to zero around times were the sensitivities of the solid displacement are experiencing negligible change in time. This indicates moments at which the load has been fully transferred to the strain and the solid has reached an equilibrium which is consistent with experimental results [13].

While the magnitudes of the sensitivities were not monotonic with respect to $\hat{\eta}$, we were still able to observe a correlation between the value of $\hat{\eta}$ and the extent and speed at which the sensitivities responded to changes in the direction $\bar{P}$ as well as the maximum magnitude they obtained. For these reasons, we do believe $\hat{\eta}$ will work better as a control parameter than the measure of structural viscosity $\delta = \lambda_v + 2\mu_v$ that was studied in [1, 2]. This is due to the complex behavior the sensitivities with respect to boundary traction displayed depending upon the range of δ [1]. Interestingly, while $\hat{\eta}$ does itself contain δ, it is also dependent upon the length L of the domain and the permeability K_0. Here, we have only considered constant permeability, however the dependence of $\hat{\eta}$ upon K_0 suggests that taking the permeability K to be nonlinear (which is often more physically relevant) may result in interesting behaviors. Considering the case of nonlinear permeability K is currently a work in progress.

Finally, our analysis shows which directions $\bar{P}$ will result in the most significant changes in $\hat{u}, \hat{p}$, and $\hat{v}$. In particular, we can increase the sensitivity for $\hat{u}$ by keeping the direction $\bar{P}$ nonzero and not changing the sign of its slope. On the other hand, $\hat{p}$ and $\hat{v}$ are most sensitive to directions $\bar{P}$ that are always changing. This tells us that while the solid displacement will remain sensitive to a load as long as it is being applied, the fluid pressure and discharge velocity lose sensitivity over time unless the force of the load itself is being changed.

7. ACKNOWLEDGMENTS

Dr. Bociu has been partially supported by NSF CAREER DMS-1555062.

REFERENCES

[1] H.T. Banks, K. Bekele-Maxwell, L. Bociu, M. Noorman and G. Guidoboni, Sensitivity analysis in poro-elastic and poro-visco-elastic models with respect to boundary data, *Quart. Apply. Math.* **75** (2017), 697–735.

[2] H.T. Banks, K. Bekele-Maxwell, L. Bociu, M. Noorman and G. Guidoboni, Local sensitivity via the complex-step derivative approximation for 1-D poro-elastic and poro-visco-elastic models, *Mathematical Control and Related Fields*, submitted 2017.

[3] H.T. Banks, K. Bekele-Maxwell, L. Bociu, M. Noorman and K. Tillman, *The complex-step method for sensitivity analysis of non-smooth problems arising in biology*, Eurasian Journal of Mathematical and Computer Applications **3** (2015), 15-68.

[4] H.T. Banks, K. Bekele-Maxwell, L. Bociu, C. Wang, *Sensitivity via the complex-step method for delay differential equations with non-smooth initial data*, CRSC-TR16-09, Center for Research in Scientific Computation, N. C. State University, Raleigh, NC, July, 2016, Quarterly of Applied Mathematics November 2, 2016. http://dx.doi.org/10.1090/qam/1458.

[5] L. Bociu, G. Guidoboni, R. Sacco and J. Webster, Analysis of nonlinear poro-elastic and poro-visco-elastic models, *Arch. Ration. Mech. Anal.* **222** (2016), 1445–1519. https://doi.org/10.1007/s00205-016-1024-9

[6] M.R. DiSilvestro and J.-K. F. Suh, Biphasic poroviscoelastic characteristics of proteoglycan-depleted articular cartilage: simulation of degeneration, *Annals of Biomedical Engineering* **30** (2002), 792–800. https://doi.org/10.1114/1.1496088

[7] J. N. Lyness, *Numerical algorithms based on the theory of complex variables*, Proc. ACM 22nd Nat. Conf., **4** (1967), 124 - 134.

[8] J. N. Lyness and C. B. Moler, *Numerical differation of analytic functions*, SIAM J. Numer. Anal., **4** (1967), 202 - 210.

[9] A.F. Mak, The apparent viscoelastic behavior of articular carilage - the contributions from the intrinsic matrix viscoelasticity and interstitial fluid flows, *J. Biomech. Eng.* **108** (1986), 123–130. https://doi.org/10.1115/1.3138591

[10] Joaquim R. R. A. Martins, Ilan M. Kroo, and Juan J. Alonso. *An automated method for sensitivity analysis using complex variables*, AIAA Paper 2000-0689 (Jan.), 2000.

[11] Joaquim R. R. A. Martins, Peter Sturdza, and Juan J. Alonso. *The complex-step derivative approximation*, Journal ACM Transactions on Mathematical Software (TOMS), 2003.

[12] L.A. Setton, W. Zhu and V.C. Mow, The biphasic poroviscoelastic behavior of articular cartilage: role of the surface zone in governing the compressive behavior, *J. Biomech.* **26** (1993), 581–592. https://doi.org/10.1016/0021-9290(93)90019-B

[13] M.A. Soltz and G.A. Ateshian, Experimental verification and theoretical prediction of cartilage interstitial fluid pressurization at an impermeable contact interface in confined compression, *J. Biomech.* **31** (1998), 927–934. https://doi.org/10.1016/S0021-9290(98)00105-5

[14] J.-K. Suh and S. Bai, Finite element formulation of biphasic poroviscoelastic model for articular cartilage, *J. Biomech. Eng.* **120** (1998), 195–201. https://doi.org/10.1115/1.2798302

[15] M. Verri, G. Guidoboni, L. Bociu and R. Sacco, The role of structural viscoelasticity in deformable porous media with incompressible constituents: applications in biomechanics, *Math. Biosci. Eng.* **15** (2018), 933–959. https://doi.org/10.3934/mbe.2018042